DIRECT AND INDIRECT SNAPPING BEHAVIORS OF SHALLOW TRUSS MODELS

Seung-Deog KIM[1], Tetsuyuki TANAMI[2]
and Yasuhiko HANGAI[3]

INTRODUCTION

In this paper, dynamic snapping behaviors are investigated by using shallow truss models under the step load, the sinusoidal load and the earthquake excitation in the up-and-down direction in order to grasp the frequency-dependent characteristics between structures and loads. To treat direct and indirect snapping, two types of models which reveal the snap-through buckling and the bifurcation buckling, respectively, under the static load are used. The influence of damping on the snapping buckling load is also examined.

ANALYTICAL MODELS

Let us consider a shallow truss structure shown in Fig.1 as an analytical model which is composed of 19 members pin-connected at 10 joints. In the paper, the span (2L) along the x-coordinate, the rise (H) and the ratio of rise-to-span (μ=H/2L) are fixed as 10m, 1m and 0.1, respectively. The model whose truss members have the same cross sectional area of 11.2cm^2 is called Type-1 which reveals the snap-through buckling under the static load. In the other hand, the model in which the members designated by 'a' in Fig.1 have the cross sectional area of 1.12cm^2 and the cross sectional area of other members is 11.2cm^2 is called Type-2 which reveals the bifurcation buckling by the coupling of the symmetrical and the unsymmetrical modes under the static load.

As the properties of members, Young's modulus E = 2.1x10^{6}kgf/cm^2 and the density ρ = 7.85x10^{-3}kgf/cm^3 are used.

---

1) Graduate Student, University of Tokyo
2) Research Associate, I.I.S. University of Tokyo
3) Professor, I.I.S. University of Tokyo

STATIC BUCKLING BEHAVIORS

The load-displacement relation adopting up to the 3rd order geometrical nonlinear terms is expressed in the form;

$$K_{ri}D_i+K_{rij}D_iD_j+K_{rijk}D_iD_jD_k=F_r \tag{1}$$

in which D_j and F_r represent displacement and load components, respectively, and the rule of summation convention is used for subscripts of i,j and k. When we make the incremental equation of Eq.(1) at the equilibrium point of (D_j^0, F_r^0), the tangent stiffness matrix K_{rj} takes the following form;

$$\overline{K}_{ri}=K_{ri}+(K_{rij}+K_{rji})D_j^0+(K_{rijk}+K_{rjki}+K_{rkij})D_j^0D_k^0 \tag{2}$$

Fig.2 show the load-displacement curves which are obtained by the displacement incremental method for the models subjected to the same vertical loads applied at two vertex nodes 1 and 2 in Fig.1. In these figures, the solid lines denote the load-displacement curves and the dotted lines represent the determinant of the tangent stiffness matrix given in Eq.(2). In the case of Type-1, there is one point of $|K_{rj}|=0$ which corresponds to the snap-through buckling point (denoted by 'A' in the figure). On the other hand, Type-2 has two points of $|K_{rj}|=0$ which represent the bifurcation buckling point (denoted by 'B') and the snap-through buckling point (denoted by 'A'). In this case, the ratio λ of the bifurcation buckling load to the snap-through buckling load is $\lambda=0.69$.

In the sequel, the load level P is normalized by the snap-through buckling load ${}_sP_{cr}$ as $\lambda=P/{}_sP_{cr}$ to discuss the numerical results.

NATURAL VIBRATION

Fig.3 shows the natural frequencies and the corresponding mode shapes for free vibration. The first two modes denote the antisymmetric and the symmetric modes in the vertical direction, respectively. The ratios of the 1st natural frequency f_1 to the 2nd one f_2 are about 1.0 for Type-1 and about 1.5 for Type-2.

Fig.4 shows the backbone curves which represent the curves between the frequency and the load level. From these figures, softening properties of the first two modes are observed. The below figures in Fig.4 show the magnification

figure of the first two modes. The 3rd, 4th and 5th natural frequencies are almost constant with the increase of λ.

DYNAMIC SNAPPING BEHAVIORS

In this section, dynamic snapping behaviors under the step load of infinite duration, the sinusoidal load and the earthquake load are examined. Nonlinear responses are numerically analyzed by Newmark's β method of $\beta=1/4$. In the analysis, the time interval of 0.01T and the time duration of 50T are used where T represents the 1st natural period for each model.

(1) STEP LOAD

Fig.5 shows the maximum vertical displacements of nodes 1 and 2 obtained from the time history curves with the increase of the load level. Solid and dotted lines represent the response with damping coefficient of h=0.0 and h=0.05, respectively. If we define the dynamic buckling load as the load level at which the maximum displacement increases suddenly, then $\lambda=0.74$ for h=0.0 and $\lambda=0.82$ for h=0.05 in the case of Type-1, and $\lambda=0.45$ for h=0.0 and $\lambda=0.70$ for h=0.05 in the case of Type-2.

For Type-1, Fig.6(a) and (b) show the time histories of displacement components (u, v and w) for the load levels of $\lambda=0.1$ and $\lambda=0.8$, respectively. It can be observed in Fig.6(b) that the direct snapping which is characterized by the vibration of large amplitude from the initial state occurs.

For Type-2, Fig.7(a) and (b) show the time histories of displacement components (u, v and w) for the load levels of $\lambda=0.1$ and $\lambda=0.5$, respectively. In this case, the dynamic snapping occurs suddenly after repeating the stable vibration with the small amplitude. This type of the dynamic snapping is called "Indirect Snapping" because of the existence of the coupling of two modes.

Fig.8 and Fig.9 show the displacement spectra of Type-1 and Type-2, respectively, under the step load. In the case of direct snapping shown in Fig.8, the dominant frequencies of displacement components u and v are, respectively, 128Hz and 156Hz which correspond to the 3rd and the 4th natural vibration modes as shown in Fig.4(a). These dominant frequencies have the similar values for $\lambda=0.1$ in the pre-buckling load level and $\lambda=0.8$ in the post-buckling load level. In the

other hand, the dominant frequencies of the vertical displacement w are different between the load levels of λ=0.1 and λ=0.8 because the backbone curves of the 2nd symmetric mode changes with the increase of the load level as shown in Fig.4(a). Namely, the 2nd symmetric mode with 39Hz is dominant at λ=0.1, but, a lot of modes given by the inter-fold of 11.2Hz exist for λ=0.8.

In the case of the indirect snapping for Type-2, Fig.9(a) and (b) show the displacement spectra for the load levels of λ=0.1 and λ=0.5, respectively. The dominant frequencies of the displacement component u are a pair of about 20Hz and 150Hz, which corresponds the 1st and the 4th modes, respectively. For the vertical displacement component w, the dominant frequency of 29Hz which corresponds to the 2nd mode for the load level of λ=0.1 changes into about 20.6Hz for the post-buckling load level of λ=0.5. At the load level of λ=0.5, the 1st and the 2nd frequencies are about 15Hz and 25Hz from Fig.4(b). The dominant frequency of 20.6Hz in Fig.9(b) can be estimated by the coupling frequency of these two modes as (15+25)/2=20Hz.

(2) SINUSOIDAL LOAD

The sinusoidal load of $F=F_0\sin\alpha\omega_0 t$ in the vertical direction is applied simultaneously to the nodes 1 and 2 in which ω_0 is the 1st angular frequency of each model.

Fig.10 and 11 show the nonlinear response curves for Type-1 and Type-2, respectively. In the linear response, the resonance occurs for α=1.0, but, in the nonlinear case, the monotonous increase of displacement response is prevented by the softening effect shown in Fig.4. For Type-1, the complete symmetric vibration is kept even in the post-buckling load level of λ=0.2 shown in Fig.10(b). For Type-2, complicated coupling behaviors can be observed.

Fig.16 and 17 show the dynamic buckling loads for Type-1 and Type-2, respectively, where solid lines represent the sinusoidal load cases. As compared with the step load, the frequency-dependent characteristics can be observed.

(3) EARTHQUAKE LOAD

Fig.12 show the time history of earthquake acceleration observed on December 17, 1987 in Chiba (Magnitude=6.7), and Fig.13 show the Fourier spectrum of this earthquake wave,

which has a dominant frequency of 7.324Hz. In the numerical analysis, the position of the dominant frequency is changed by the extension or the contraction of the time interval by introducing the parameter of β. In the case of β=1, the dominant frequency of the earthquake wave corresponds to the 1st natural frequency of each model.

Fig.14 and 15 show time histories of displacement component w with β=0.9 for Type-1 and β=1.5 for Type-2. The dynamic buckling loads are depicted in Figs. 16 and 17 by dotted lines.

CONCLUSION

In this paper, dynamic snapping behaviors are investigated by using shallow truss models under the three kinds of loads : the step load, the sinusoidal load and the earthquake load. The numerical results show the strong frequency-dependent characteristics between structures and loads about the dynamic buckling load.

REFERENCES

[1] Lock,M.H., Okubo,S. and Whittier,J.S., "Experiments on the snapping of a shallow dome under a step pressure load," AAIA Journal, Vol.6, No.7, 1968, pp.1320-1326.

[2] TANAMI,T. and HANGAI,Y., "Dynamic buckling behaviors of reticulated single-layer dome model to up-and-down earthquake excitations," Bulletin of Earthquake Resistant Structure Research Center, No.22, 1989, pp.109-125.

[3] KIM,S.D., TANAMI,T. and HANGAI,Y., "Dynamic buckling of shallow structures due to up-and-down excitations," Japan NCTAM, 1989, pp.59-60.

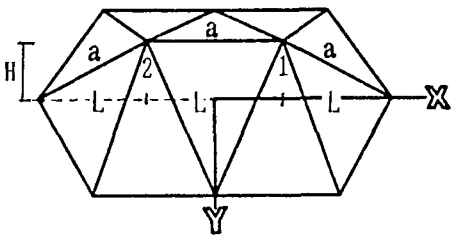

Fig.1 : Analytical model

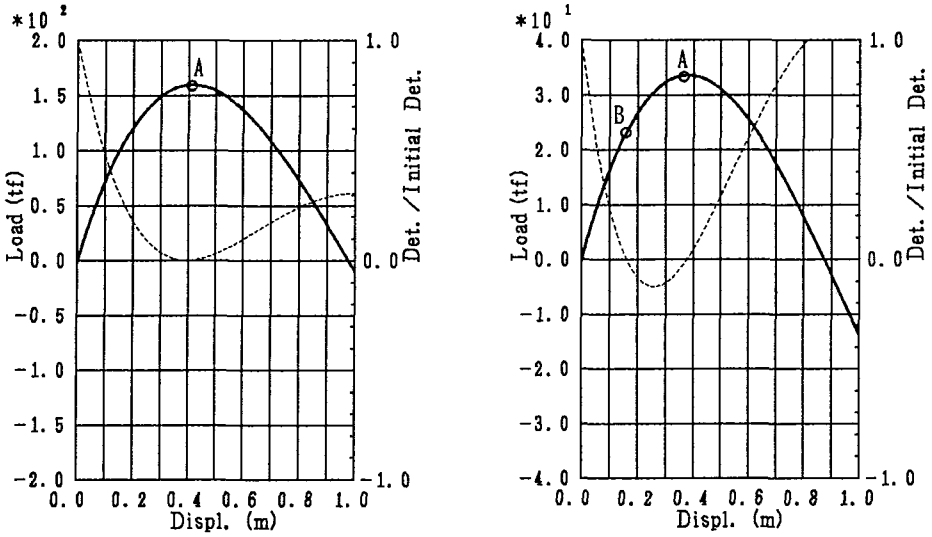

(a) Type-1 (b) Type-2

Fig.2 : Load-displacement curves and determinant of tangent stiffnees matrixes

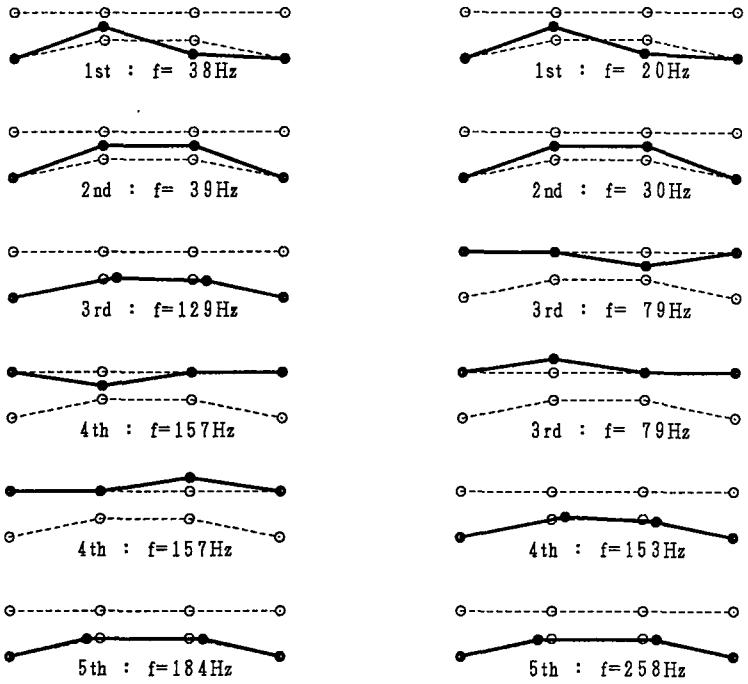

(a) Type-1 (b) Type-2

Fig.3 : Natural vibration modes

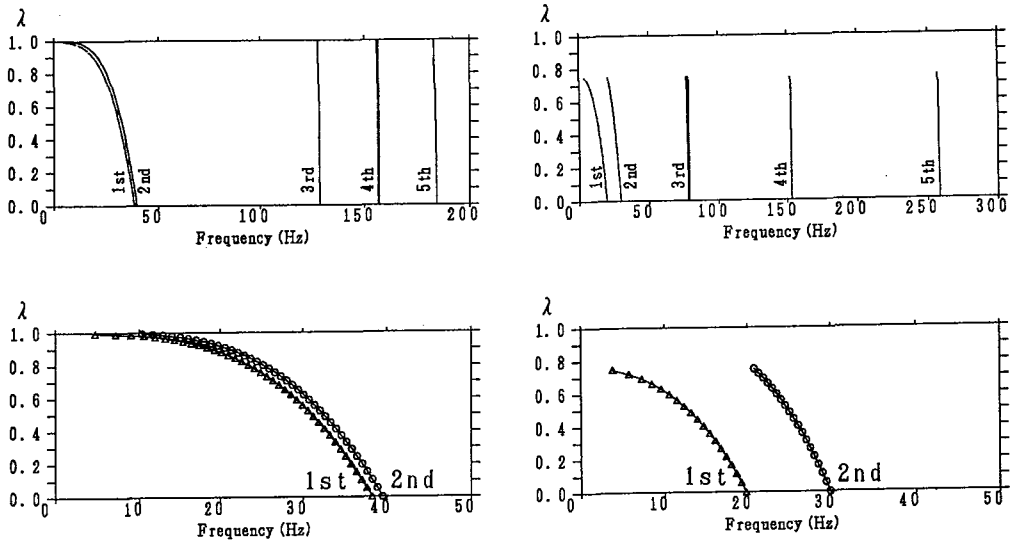

(a) Type-1　　(b) Type-2

Fig.4 : Backbone curves

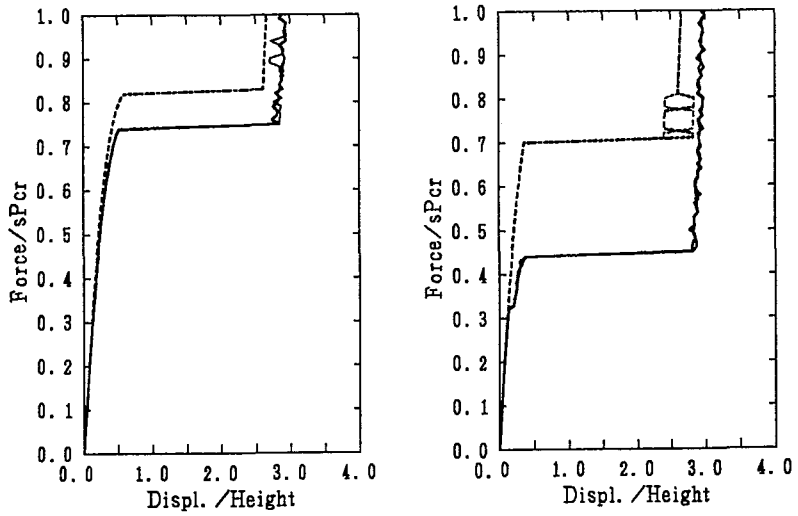

(a) Type-1　　(b) Type-2

Fig.5 : Maximum displacement responses under step load

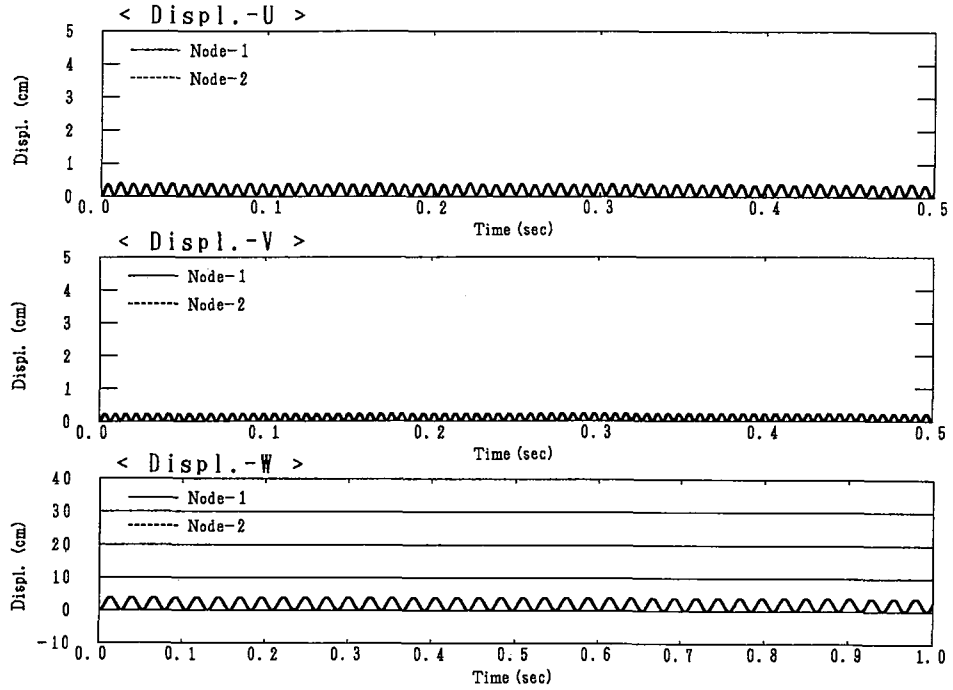

(a) Pre-buckling load level(λ=0.1)

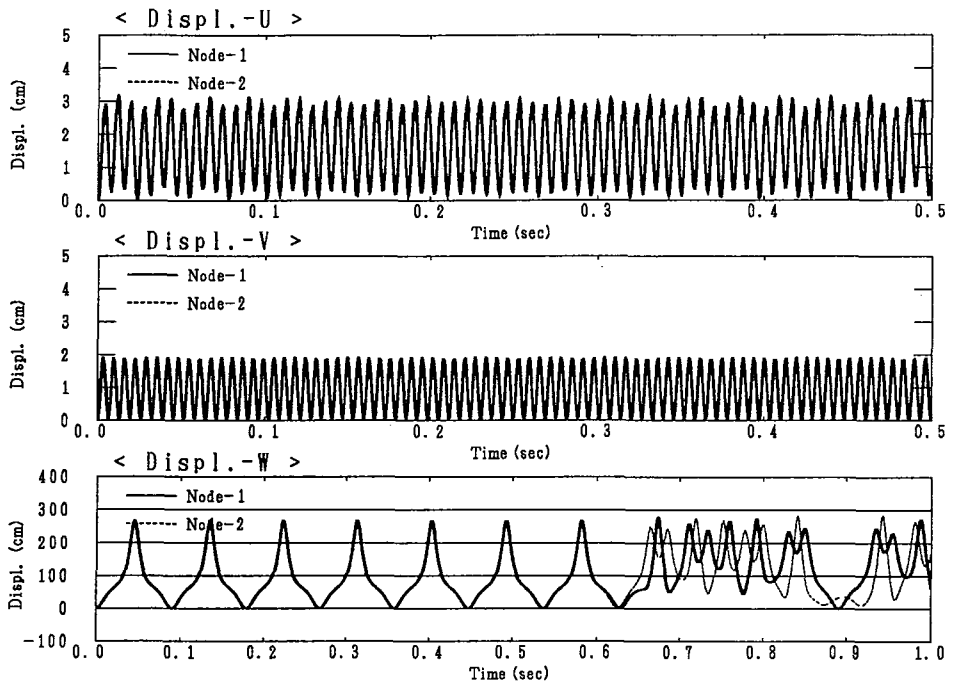

(b) Post-buckling load level(λ=0.8)

Fig.6 : Time history curves of Type-1 under step load

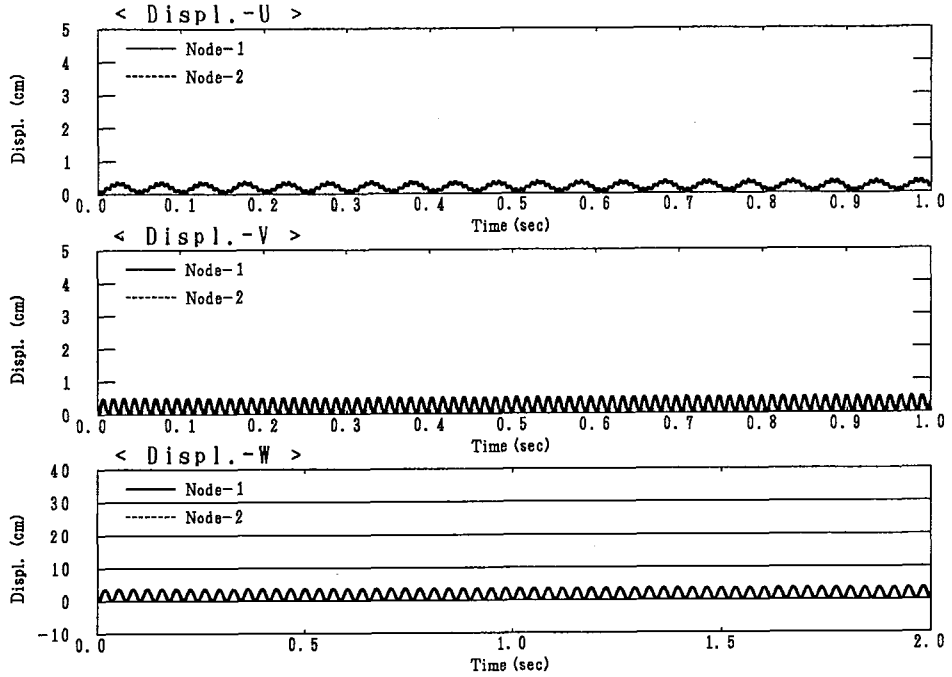

(a) Pre-buckling load level(λ=0.1)

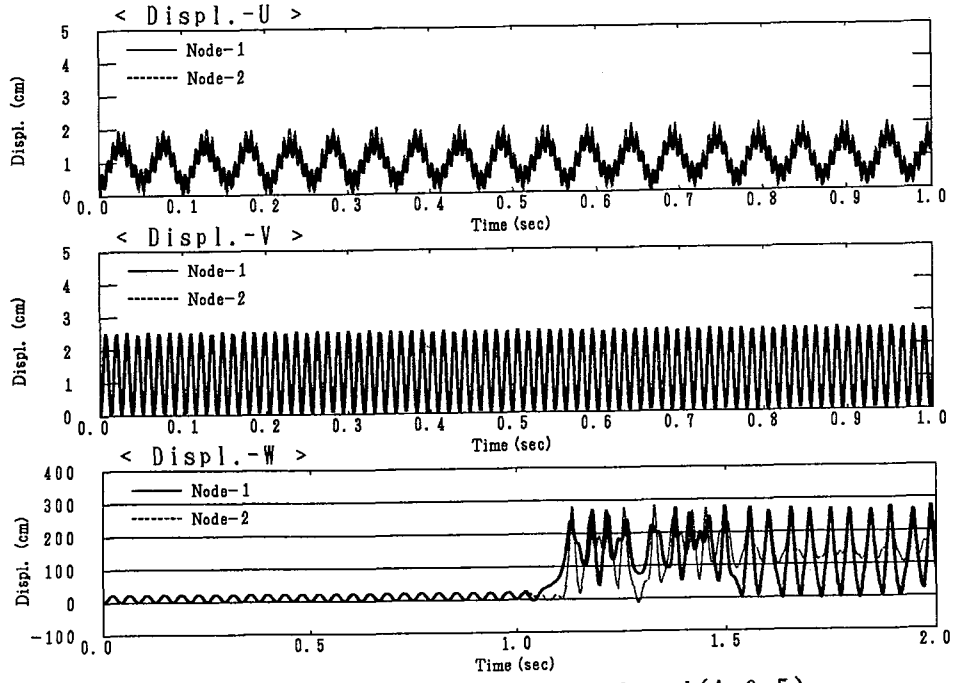

(b) Post-buckling load level(λ=0.5)

Fig.7 : Time history curves of Type-2 under step load

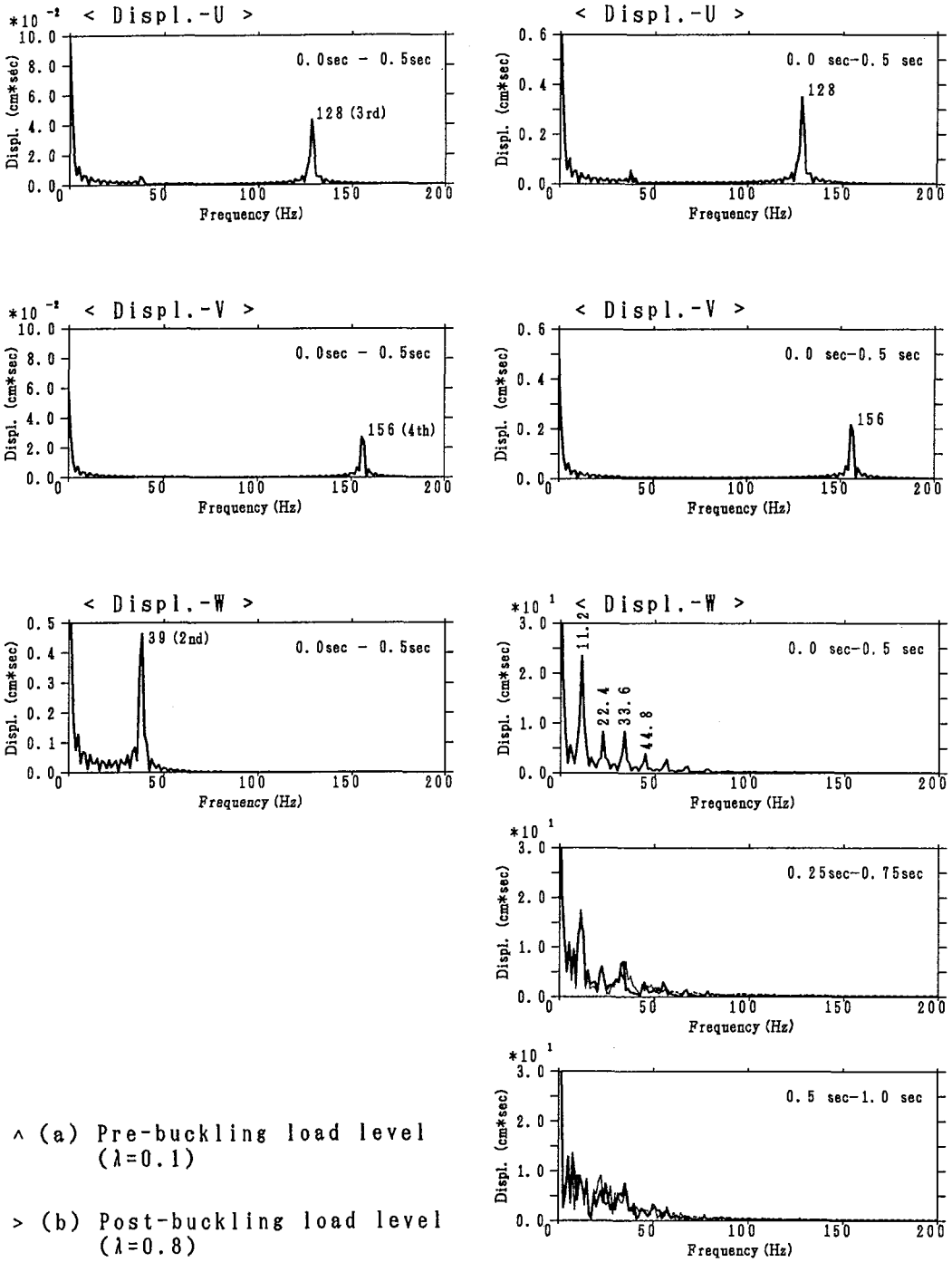

^ (a) Pre-buckling load level (λ=0.1)

> (b) Post-buckling load level (λ=0.8)

Fig.8 : Displacement spectra of Type-1 under step load

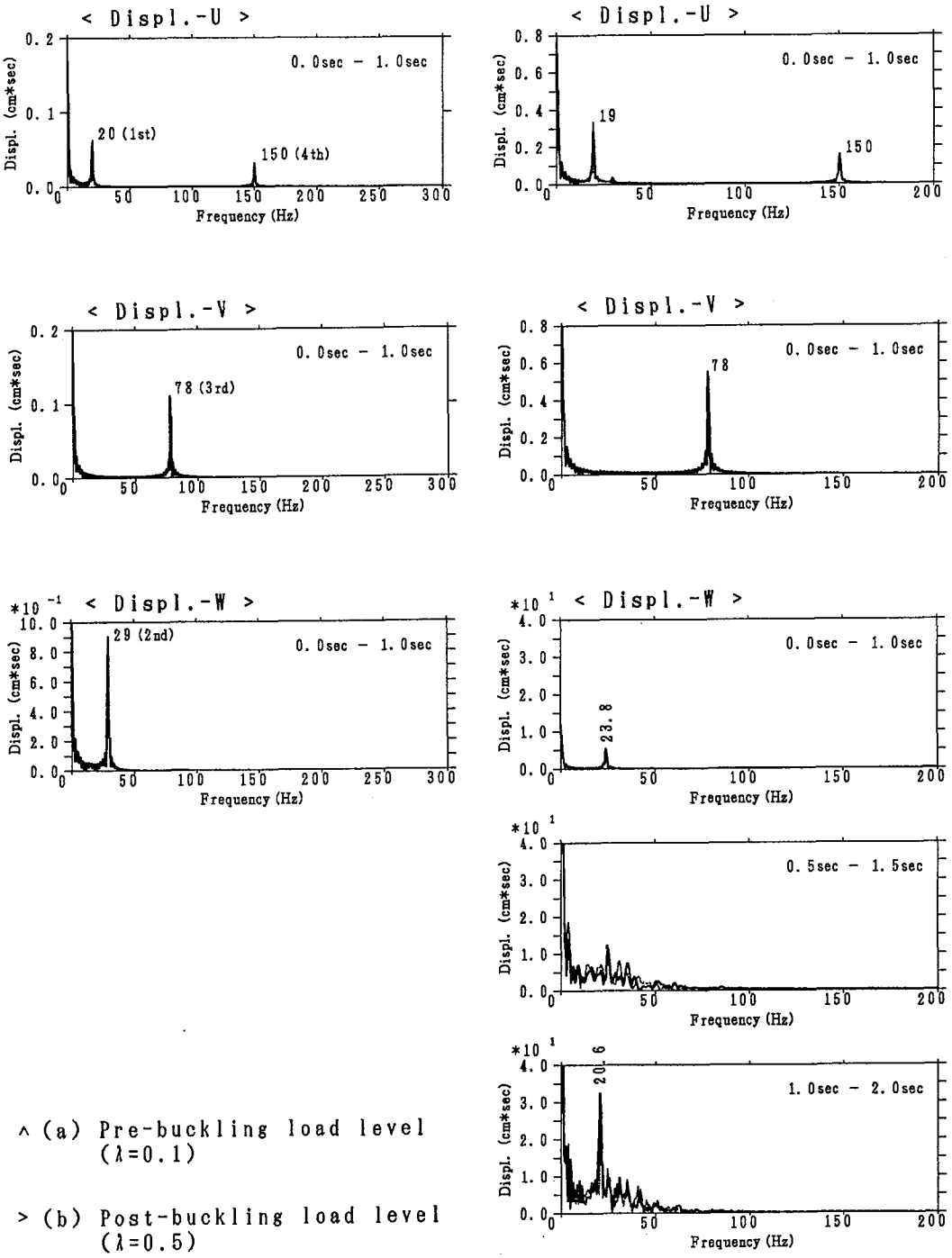

^ (a) Pre-buckling load level (λ=0.1)

> (b) Post-buckling load level (λ=0.5)

Fig.9 : Displacement spectra of Type-2 under step load

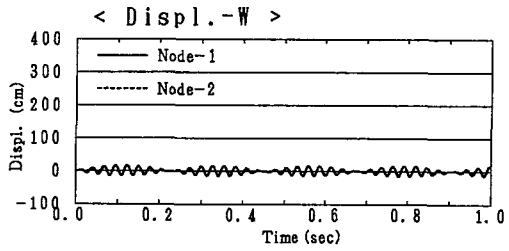

(a) Pre-buckling load level
(α=0.9, λ=0.1)

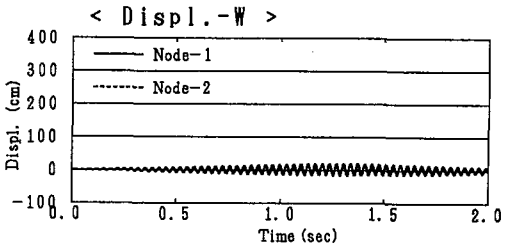

(a) Pre-buckling load level
(α=1.5, λ=0.01)

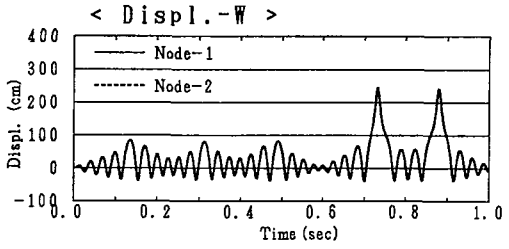

(b) Post-buckling load level
(α=0.9, λ=0.2)

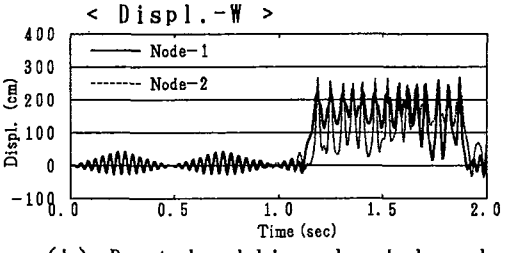

(b) Post-buckling load level
(α=1.5, λ=0.1)

^ Fig.10 :
Time history curves of Type-1
under sinusoidal excitation

> Fig.11 :
Time history curves of Type-2
under sinusoidal excitation

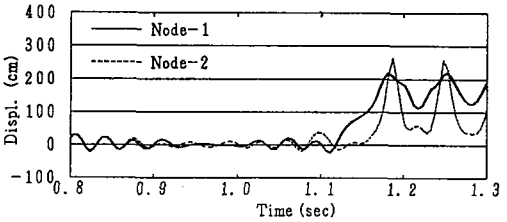

(c) Magnified figure of (b)

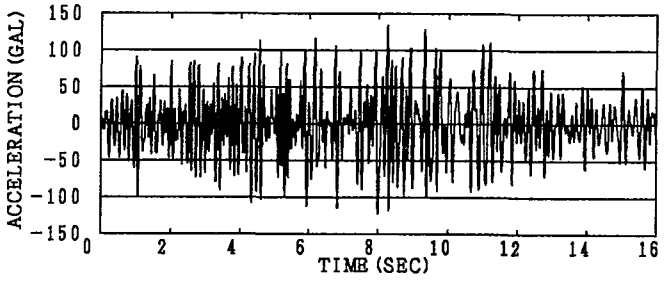

Fig.12 : Earthquake wave

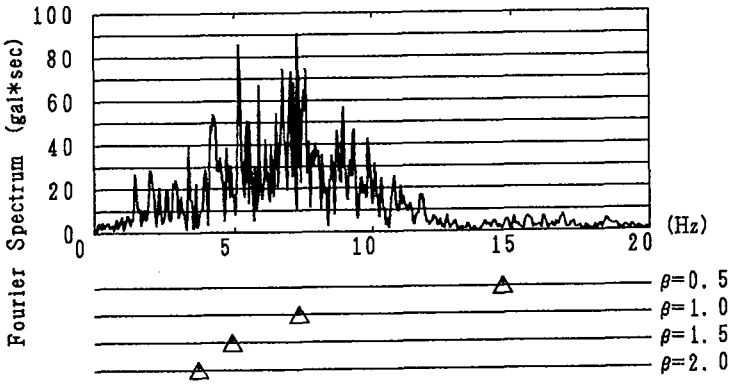

Fig.13 : Fourier spectrum of earthquake wave

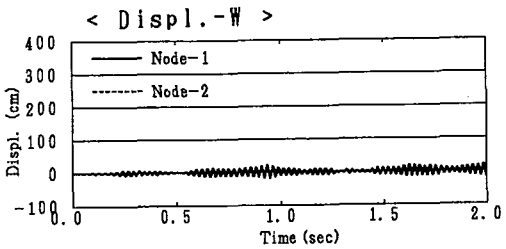

(a) Pre-buckling load level
(β=0.9, λ=0.1)

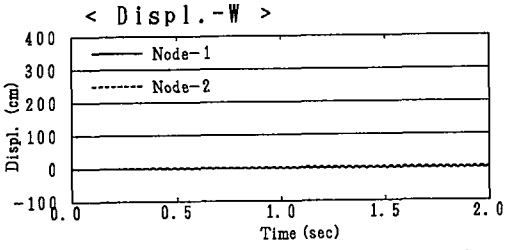

(a) Pre-buckling load level
(β=1.5, λ=0.01)

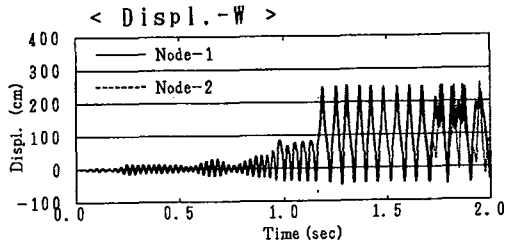

(b) Post-buckling load level
(β=0.9, λ=0.2)

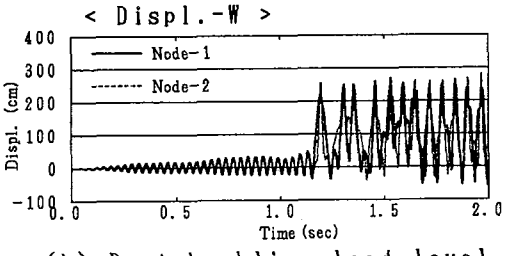

(b) Post-buckling load level
(β=1.5, λ=0.1)

^ Fig.14 :
Time history curves of Type-1
under earthquake excitation

> Fig.15 :
Time history curves of Type-2
under earthquake excitation

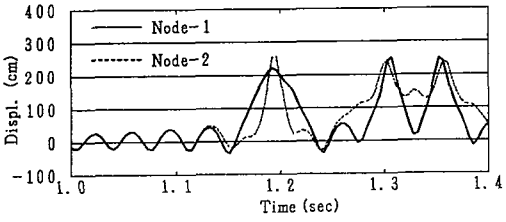

(c) Magnified figure of (b)

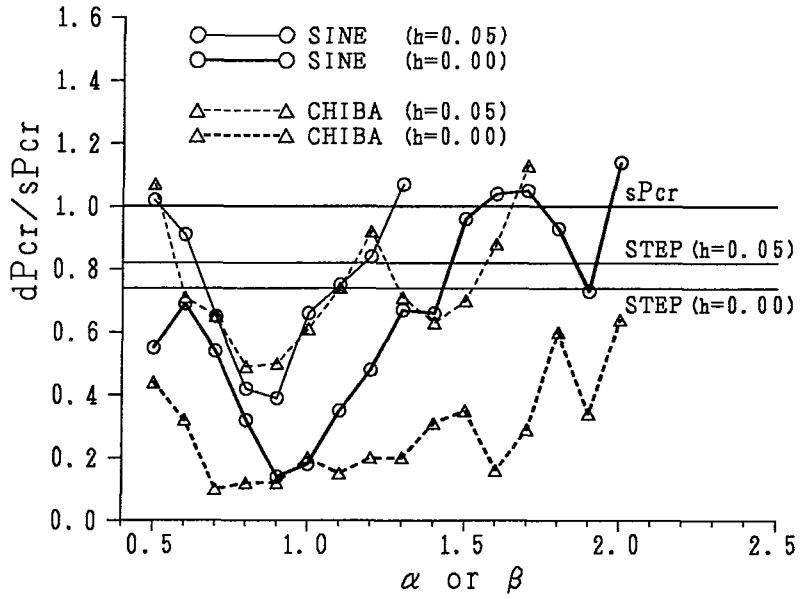

Fig.16 : Comparison of dynamic buckling loads of Type-1

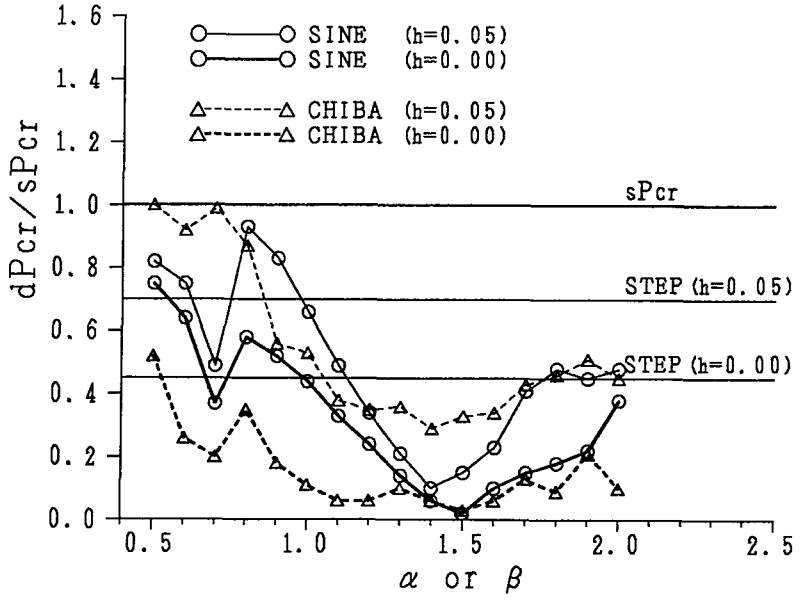

Fig.17 : Comparison of dynamic buckling loads of Type-2